Multi-objective optimization of turbo-ORC systems for waste heat recovery on passenger car engines

Kévin Rosset*, Violette Mounier, Eliott Guenat, Jürg Schiffmann

kevin.rosset@epfl.ch, violette.mounier@epfl.ch, eliott.guenat@epfl.ch, jurg.schiffmann@epfl.ch

Ecole Polytechnique Fédérale de Lausanne, Laboratory for Applied Mechanical Design,
Rue de la Maladière 71b, 2002 Neuchâtel, Switzerland

* Corresponding Author

ABSTRACT

Waste heat recovery from passenger car internal combustion engines by means of an organic Rankine cycle (ORC) system is promising for reducing CO_2 emissions. In this study, different cycle configurations capable of converting waste heat from both coolant and exhaust gases are investigated based on different working fluid categories. Radial-inflow turbines are considered as expansion devices and corresponding isentropic efficiencies are evaluated based on a preliminary design map accounting for the effect of the pressure ratio. Mechanical losses resulting from the use of a gas-bearing-supported rotor driving a permanent magnet generator are also evaluated. In order to identify the turbo-ORC system design tradeoffs, constrained multi-variable and multi-objective optimizations are performed using an evolutionary algorithm. It is found that the optimal cycle configuration and working fluid depend on the available space in the vehicle and that the condenser is the most critical component for the ORC system integration. In addition, the most suitable working fluids for this application are characterized by (1) a boiling point close to the heat sink temperature, (2) a high critical pressure, and (3) a high molecular weight. The resulting optimal radial-inflow turbines are 10-33 mm in tip diameter and operate at 80-330 krpm.

Keywords: internal combustion engine, waste heat recovery, organic Rankine cycle, turbo-generator preliminary design, heat exchanger sizing, multi-objective optimization

1. Introduction

Growing concerns about fossil fuel shortage and global warming advocate for a more rational use of primary energy. Currently, the transportation sector consumes 20% of the worldwide primary energy supply, while depending mainly (92%) on fossil fuels [1]. As a consequence, this sector is also responsible for 24% of the worldwide CO_2 emissions from fuel combustion, including 75% from road transports [2]. In the European Union, passenger cars account for 87% of the total road vehicle fleet while producing 64% of the associated CO_2 emissions [3]. These high levels of emissions result from the low fuel-to-wheel efficiency of vehicles propelled by internal combustion engines (ICE), i.e. typically 15-31% [4]. There is consequently a strong potential for energy savings and emission reductions by improving the efficiency of ICE-powered road vehicles. Such improvements can be achieved by (1) decreasing the vehicle power requirements, (2) improving the efficiency of the power transmission train, and (3) integrating advanced engine technologies [5]. In order to encourage innovations for cleaner vehicles, the European Union gradually imposes "emission performance standards" to vehicle manufacturers, with the ultimate goal of reducing the average CO_2 emissions of passenger cars to 95 g/km by 2020 [6]. In the recent years, waste heat recovery (WHR) technologies have been investigated in order to further increase the efficiency of ICE-powered vehicles. Indeed, for a given fuel input, two thirds of the energy is lost as heat in the engine coolant and exhaust gases [7]. Among engine WHR technologies, Organic Rankine Cycle (ORC) systems offer the most attractive combination of simplicity, component cost and efficiency, with a fuel economy improvement potential around 10% and a payoff time within 2-5 years [8].

The ORC is a versatile concept which can be combined with numerous applications [9] by properly selecting the working fluid, tuning the cycle design parameters and possibly considering regeneration [10,11]. When several heat sources are available, the cycle configuration can be adapted accordingly. Two heat sources at different temperature levels can be exploited through series [12-15] or parallel [15-17] evaporators, series evaporators with intermediate regeneration or two-stage regeneration [18], parallel evaporators with different pressure levels (dual-pressure) and two-stage pumping and expansion [19,20], or even through cascade (dual-loop) cycles with two different working fluids [21,22] and regeneration [23]. With regards to the selection of the working fluid, not only its thermodynamic properties are important, but also [24] the thermal stability [25-29] especially in the presence of petroleum-based lubricants [30], material compatibility [31], environmental impact, toxicity, flammability, availability and cost. Depending on the application and specifications, the working fluid selection can vary significantly. As a matter of fact, one working fluid may maximize the thermodynamic efficiency while another one reduces the heat exchanger size and cost or simplifies the expander design [9].

For engine waste heat recovery applications, the ORC system efficiency is primarily influenced by the working fluid and the expander that are selected [8]. While small-scale cost-effective screw and scroll expanders can be retrofitted from volume-produced refrigeration compressors, their limited built-in volume ratios prevent their use in high-expansion-ratio and high-temperature systems [9]. Nevertheless, the scroll expander is the most widely experimented ORC volumetric expander in the literature [32], with isentropic efficiencies up to 86% [33]. Screw expanders can also reach high isentropic efficiencies (up to 88%) [34] but are characterized by higher rotational speeds than scroll expanders, as well as challenging manufacturing tolerances when applied in 10 kW or lower scale systems [32]. In order to achieve higher expansion ratios, reciprocating expanders and in particular the swash-plate type [35] are well indicated. However, they are less efficient, complex and consequently expensive [32]. Although they suffer from high leakage and friction losses, vane expanders are a low cost solution for 1 kW or lower scale systems [32]. Recently, a 2 kW vane expander has been successfully tested in an ORC system bottoming a light-duty vehicle engine, with a peak overall efficiency of 53% [36-38]. Positive displacement expanders are further characterized by a volumetric efficiency which is closely related to their lubrication [39], thus implying auxiliary systems using petroleum-based lubricants that may cause the overall system performance to drop in the long term [40].

In contrast, dynamic expanders are characterized by higher power densities, which is beneficial for mobile applications, while their working principle does not rely on a lubricant to be mixed with the working fluid. However, they are rather incompatible with wet vapor expansion (which can be avoided by a proper working fluid selection [41]), and are inherently associated with high rotational speeds at small scale [42,43]. The higher stage expansion ratio capability of radial-inflow turbines compared to axial or radial-outflow turbines makes this technology convenient for high-temperature ORC applications. For instance, in the transportation sector, radial-inflow turbines are widely used as the driver of turbochargers. Nevertheless, partial-admission impulse axial turbines are also investigated for waste heat recovery from vehicle engines [44-46], despite limited isentropic efficiencies (43-57%). Due to increased friction, mixing and tip-clearance losses [47], small-scale radial-inflow turbines also present lower performances compared to their large-scale counterparts. Alshammari et al. [48] developed a novel back-swept-bladed radial-inflow turbine, which was tested in an ORC system combined with a truck engine. The prototype generated 6.3 kW at 20 krpm with a peak isentropic efficiency of 35.2%, in off-design operating conditions though. Guillaume et al. [49] tested a 3.5 kW radial-inflow turbine supported on rolling-element bearings flushed by the working fluid. The prototype was evaluated in a boiler-driven ORC system at speeds between 46 and 70 krpm, and turbine isentropic efficiencies ranging from 60 to 75% were measured. The overall turbo-generator efficiency did not exceed 28% due to high bearing losses. Moreover, the cycle thermal efficiency was negatively affected by the increased pump power resulting from supplying pressurized liquid to the bearings. On the other hand, Schiffmann and Favrat [50,51] demonstrated the technical feasibility of direct-driven high-speed organic-fluid turbomachinery supported on dynamic gas-lubricated bearings. Demierre et al. [52,53] successfully tested a compressor-turbine unit supported on

herringbone grooved journal bearings lubricated with the organic working fluid, at rotational speeds in excess of 200 krpm. Isentropic efficiencies in the range of 57-74% were measured for the 18 mm diameter radial-inflow turbine, with a power output in the range of 2.5 kW, which confirms the technical feasibility and high power density of such turbomachines.

Several approaches have been pursued for the design of ORC systems. Often, only a limited number of cycle configurations and a few arbitrary working fluids are considered. Many studies investigate ORC systems from a purely thermodynamic perspective, based on a parametric approach, assuming constant temperature pinches in the heat exchangers and constant isentropic efficiencies for the pumping and expansion devices [10-12,22,23,54,55]. Thermo-economic studies typically address technical aspects and cost based on heat exchangers area (evaluated through the LMTD method), pump power consumption, expander power output (for dynamic machines) or inlet flowrate (for volumetric machines), and possibly other components. Quoilin et al. [56] performed a parametric study suggesting that thermodynamic and economic optima do not match. Amicabile et al. [57] obtained the same result by optimizing sub- and super-critical cycles, with or without regeneration, based on 2 design variables and uniform sampling of the search space. This triggered interest for multi-variable and multi-objective optimizations based on genetic algorithms and considering different cycle configurations and working fluids for waste heat recovery applications [58,59], including truck engine bottoming [60]. Galindo et al. [61] introduced pressure-ratio-dependent isentropic efficiencies in the multi-objective optimization of a basic ORC system using ethanol as the working fluid, for passenger car applications, considering plate heat exchangers and a swash-plate expander, which model was experimentally validated. Bahamonde et al. [62] proposed a similar but more advanced methodology for designing long-haul truck engine exhaust WHR ORC systems, using a small-scale axial, radial-inflow or radial-outflow turbine. In their approach, the feasible design space is first evaluated by integrating thermodynamic cycle calculations with a simplified turbine design procedure, involving a first guess of the isentropic efficiency. In a second step, the actual optimization is performed by coupling the thermodynamic design with a 1D mean-line aerodynamic model of the chosen turbine. Applying this method, they converged to a 75 mm diameter radial-inflow turbine using siloxane MM, spinning at 90 krpm, and producing 11,6 kW with an isentropic efficiency of 77.3% at the design point.

Due to the intrinsic function of mobile ICEs, waste heat sources are of a highly transient nature and several studies suggest that the actual performance is below the expectations derived from system design and optimization performed under steady-state conditions. Based on a quasi-static evaluation over the whole operating map of a passenger car engine, Boretti [13] found that the average fuel efficiency improvement of a regenerative R245fa cycle utilizing both engine coolant and exhaust gases achieved 5.1% on average, compared to 8.2% at design point. Grelet et al. [15] compared the steady-state and transient performances of a truck engine WHR system and found that the net power output may drop by 50% in transient operation. However, they evaluated several cycle configurations and working fluids, and concluded that different system architectures could still be ranked qualitatively, even if evaluated based on a steady-state approach. Horst et al. [63] assessed the fuel savings from WHR on a passenger car engine over a dynamic motorway driving cycle in both ideal and integrated scenarios. A basic steam Rankine cycle was considered with the engine exhaust gases as heat source and the engine coolant as heat sink. The fuel consumption was reduced by 3.4% in the quasi-static scenario but only by 1.3% in the integrated dynamic scenario. The contributions to this reduction were identified as: limited power demand of the on-board electric system (33%), heat losses due to non-ideal integration of the exhaust evaporator (24%), higher rolling resistance of the vehicle resulting from increased weight (20%), higher drag resulting from active air vents (14%), increased exhaust backpressure due to the presence of the exhaust evaporator (5%) and additional power consumption of the coolant pump (4%). This clearly demonstrates the importance of further electrifying vehicles and designing compact and light WHR systems. However, these figures are based on a non-optimized cycle configuration using water, with a low-efficiency turbine (40% peak) and a simple control strategy, thus suggesting substantial improvement perspectives. Alternatively, Di Battista et al. [64] showed that the backpressure can significantly increase the fuel consumption if the exhaust evaporator is inadequately chosen. A number of authors [14,38,44,65,66] recommend shell-

and-finned-tube heat exchangers in a cross-flow arrangement, since they provide both high heat exchange areas and limited pressure drops on the exhaust gas. For the system condenser, it is effective to use a radiator (plate-fin flat-tube type) installed in the vehicle front cooling package exposed to direct air cooling, rather than a dedicated liquid-phase coolant circuit which would need to be cooled in a second radiator [15,67]. Furthermore, if space is too limited at the front of the vehicle, it turns out that regeneration can both increase the system net power output and reduce the size of the condenser, at the expense of additional weight though [67]. Many difficulties are consequently arising from transient engine operating conditions and other vehicle constraints. However, BMW [44] experimentally demonstrated that the dynamic operation of a Rankine system bottoming a passenger car engine is viable.

1.1 Nature of the issues

It is observed that there is a lack of integrated multi-variable and multi-objective optimization of waste heat recovery ORC systems for passenger car engines. In particular, a back-to-back comparison between different cycle configurations that are capable of converting both the engine coolant and exhaust gases is missing. In addition, preliminary turbine design is rarely applied in this context, although the expander specifications such as expansion ratio and mass flowrate, as well as the selected working fluid, are known to have a significant impact on the system feasibility and performance. Furthermore, the overall expander design, including the evaluation of electromechanical losses, is often neglected. As a consequence, the true system design boundaries and tradeoffs remain unexplored for this application.

1.2 Goal and objectives

The goal of this study is the identification of the tradeoffs between the ORC system output power, size and operating conditions, for passenger car engine bottoming. The objectives are to (1) assess the thermodynamic performance of single- and dual-source cycle configurations, (2) quantify the effect of the working fluid selection, (3) investigate the effect of gas-bearing-supported radial-inflow turbine, and (4) characterize the various design tradeoffs between the cycle, turbine and heat exchangers.

1.3 Scope of the paper

In order to achieve this goal, thermodynamic models are implemented for each single-loop cycle configuration proposed in the literature. The models are extended with (1) the sizing of the heat exchangers, considering a simple concentric-tube design, (2) the preliminary design of radial-inflow turbines, based on non-dimensional performance maps, and (3) the preliminary design of gas-bearing-supported rotors, including the evaluation of the corresponding mechanical losses. A representative set of environmentally friendly working fluids covering a broad range of thermodynamic properties is defined, and an optimization is performed for each pair of fluid/configuration, using an evolutionary algorithm. Maximum working fluid temperature, turbine pressure ratios and heat exchanger pinches are defined as the 5-7 input variables for the optimizer, while the system net power output and total heat exchange area are considered as the 2 objective functions. Models and assumptions are detailed in section 2 while the resulting Pareto fronts and system design tradeoffs are presented and discussed in section 3.

2. Materials and methods

2.1 Test-case vehicle engine

The considered vehicle is equipped with a 1.2 L turbocharged gasoline engine (max. 96 kW). Test data have been analyzed in order to extract waste heat flows and temperatures associated with best-efficiency regime under urban (50 km/h) and highway (120 km/h) operation on flat roads. In both operating modes, coolant and exhaust gas streams have a significant potential when compared to the

corresponding engine power output (Table 1). From an exergy point of view though, the coolant yields significantly less recoverable power than the exhaust gases, due to its lower temperature (exergy calculations in Table 1 are based on a 25°C reference temperature). Moreover, while exhaust gases could be cooled down to ambient temperatures, a limit of 150°C is imposed in order to avoid condensation and the formation of acid in the exhaust pipe [68], thus reducing the available energy and exergy rates. Since designing a vehicle WHR turbo-ORC system based on urban operation provides less efficiency improvement potential [42] and is technically more challenging compared to highway operation due to the highly dynamic character or urban traffic, this study focuses on the highway operating mode. It is noted that highway operation at 120 km/h was also the design point of the BMW Turbosteamer [44], which was applied to a passenger car engine.

Table 1: Vehicle waste heat characterized in terms of flowrate, temperature, energy and exergy rates

Vehicle operation	Engine		Exhaust gases					Coolant (MPG50)				
	Load	P_{eng}	$\dot{m}$	T_{min}	T_{hot}	$\dot{Q}$	$\dot{E}$	$\dot{V}$	T_{cold}	T_{hot}	$\dot{Q}$	$\dot{E}$
	-	kW	kg/h	°C	°C	kW	kW	L/min	°C	°C	kW	kW
Urban (50 km/h)	4%	3.80	20.9	150	425	1.66	0.76	32.2	104.5	105.5	1.99	0.42
Highway (120 km/h)	24%	22.9	86.0	150	706	14.3	7.87	48.2	101.2	105.1	11.6	2.41

2.2 Cycle configurations

In order to extract useful power from the engine waste heat, 6 cycle configurations are considered (Figure 1), all of them using the ambient air as the cooling medium for the condenser (CD) and including a regenerator (RG) by default. The first (Figure 1a) and second (Figure 1b) configurations are single-source, using the engine coolant and the engine exhaust gases as heat source for the evaporator (LTEV/HTEV) respectively. The remaining components are a pump (P) driven by a motor (M) and a turbine (T) driving a generator (G). The other configurations simultaneously exploit both waste heat sources, thus integrating a low-temperature evaporator associated with the engine coolant and a high-temperature evaporator associated with the exhaust gases. The third (Figure 1c) and fifth (Figure 1e) configurations consider series and parallel evaporators, respectively. In the series layout, engine coolant is primarily used to preheat the working fluid before it is evaporated by the engine exhaust gases, while in the parallel layout, both heat sources evaporate the working fluid, thus limiting the evaporation temperature to a value that is lower than the engine coolant temperature. The fourth configuration (Figure 1d) extends the third one by adding a second regenerator (HTRG) between the two evaporators, which provides a significant thermal efficiency improvement potential and is also inherently advantageous under varying engine operating conditions, according to Kim et al. [18]. Finally, the sixth configuration (Figure 1f) extends the fifth one by further compressing the working fluid upstream of the high-temperature evaporator and by realizing the expansion over two turbine stages (LPT/HPT). According to Panesar [19] and Chen et al. [20], this configuration has a significant thermal efficiency improvement potential. In order to make it more cost-effective though, the two turbine stages are directly coupled to the same electrical generator, hence constraining them to rotate at the same speed. Dual-loop configurations are not considered as a result of their higher complexity/cost and owing to their lower performance and larger heat exchangers area/volume compared to an equivalent dual-pressure configuration [19,20]. This cost-benefit reasoning was also adopted by BMW for their Turbosteamer [44].

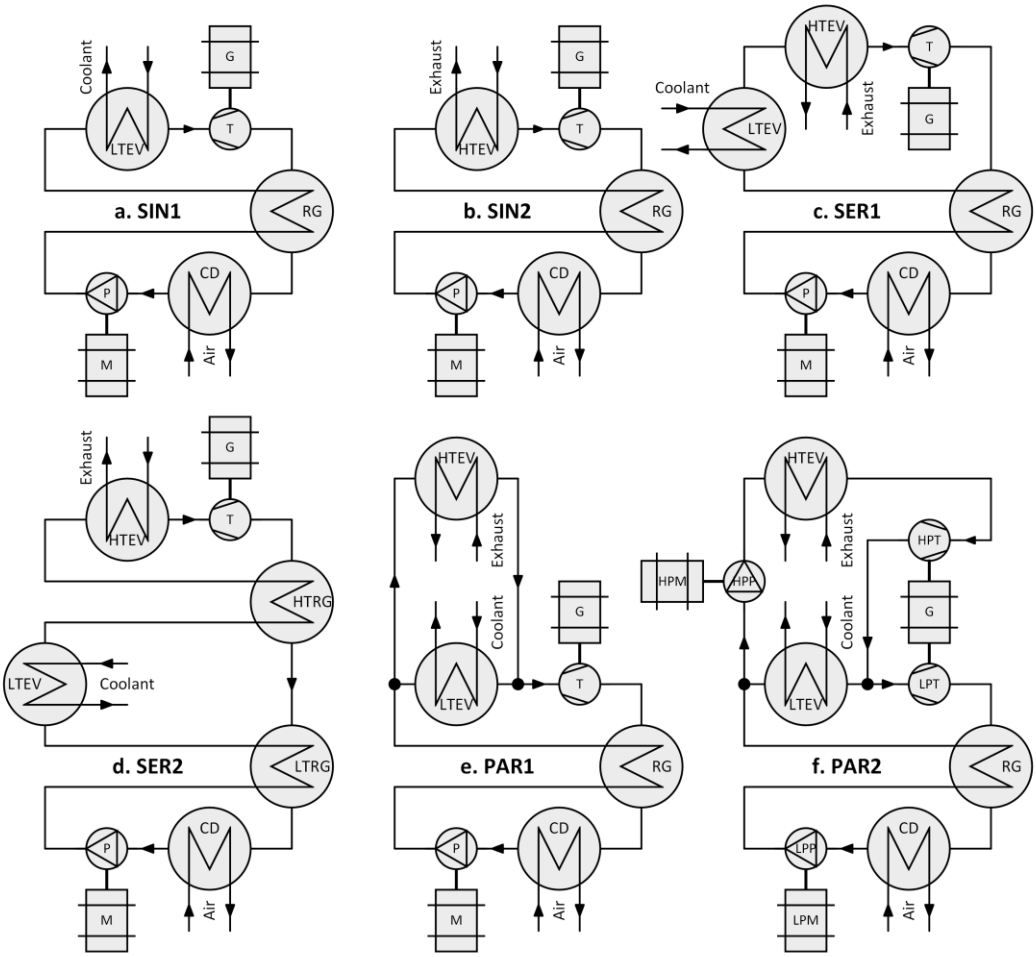

Figure 1: Considered cycle configurations:
a. Single-source using coolant, b. Single-source using exhaust gases, c. Dual-source with series evaporators, d. Dual-source dual-regeneration (with series evaporators), e. Dual-source with parallel evaporators, f. Dual-source dual-pressure (with parallel evaporators)

2.3 Working fluids

In order to provide a sufficient level of generality without evaluating a large number of working fluids, only ten are investigated (Table 2). The fluids, however, are selected such as to cover a wide range of chemical classes and thermodynamic properties. The selected working fluids include one alcohol, two hydrocarbons (HC), two aromatic hydrocarbons, three hydro(chloro)fluoroolefins (H(C)FO), one hydrofluoroketone (HFK), one siloxane, with molecular weights ranging from 46 to 316 g/mol, boiling points from -19 to 111°C, critical temperatures from 109 to 319°C, critical pressures from 19 to 63 bar, and slope of the saturated vapor curve from -2.9 to 2.7 J/(kgK^2). The slope of the saturated vapor curve $\xi = ds/dT$ characterizes the tendency of the working fluid to become drier ($\xi > 1$) or wetter ($\xi < 1$) while expanding [24] and is calculated in Table 2 as an average from 300 K to 90% of the critical temperature. The fluid selection was performed based on environmental criteria, namely zero ozone depletion potential (ODP) and low global warming potential (GWP). The fluid properties are summarized in Table 2, including an indicative value for their thermal stability limit (maximum operational temperature) in contact with stainless steel. It should be noted that ethanol, butane, pentane, benzene, toluene and MM are flammable, with auto-ignition temperatures ranging from 270 to 500°C [69], while the other fluids are characterized by a low flammability according to the ASHRAE Standard 34 [70]. In order to retrieve the thermodynamic and transport properties of the working fluids for the system simulations, a software library [71] is used.

Table 2: Selected working fluids and their general properties [71]

#	Fluid	Class	m g/mol	T_{boil} °C	T_{crit} °C	P_{crit} bar	$\bar{\xi}$ J/(kgK^2)	T_{max} °C	GWP
1	Ethanol	Alcohol	46.1	78.4	241.6	62.7	-2.90	N/A	N/A
2	n-Butane	HC	58.1	-0.5	152	38	1.04	< 310 [27]	3 [17]
3	n-Pentane	HC	72.1	36.1	196.6	33.7	1.81	315 [29]	7 [17]
4	Benzene	Arom. HC	78.1	80.1	288.9	49.1	0.52	N/A	N/A
5	Toluene	Arom. HC	92.1	110.6	318.6	41.3	1.05	400 [29]	N/A
6	R1234ze(E)	HFO	114	-19	109.4	36.3	0.12	N/A	6 [72]
7	R1233zd(E)	HCFO	130.5	18.3	166.5	36.2	0.36	200 [25]	1 [25]
8	R1336mzz(Z)	HFO	164.1	33.4	171.3	29	0.82	250 [25]	2 [25]
9	Novec 649	HFK	316	49.1	168.7	18.7	1.63	300 [73]	1 [73]
10	MM	Siloxane	162.4	100.3	245.6	19.4	2.69	300 [26]	N/A

2.4 Thermodynamic cycle model

In order to assess the WHR potential of the proposed Rankine cycles, steady-state thermodynamic models have been implemented for each cycle configuration. Mass and energy conservation laws are applied under the assumptions of 1D flow, negligible kinetic and potential energy variations, isobaric heating and cooling processes, and perfectly insulated heat exchangers. Model inputs are summarized in Table 3. Turbine pressure ratios, heat exchanger pinches, and maximum working fluid temperature are defined as input variables for the optimization process. While the maximum temperature input is required for all the configurations, single-source configurations (SIN1, SIN2 in Figure 1) rely on 1 pressure ratio and 3 pinches, dual-source single-pressure configurations (SER1, SER2, PAR1) on 1 pressure ratio and 4 pinches, and the dual-source dual-pressure configuration (PAR2) on 2 pressure ratios and 4 pinches. Except for the PAR1 configuration, the maximum working fluid temperature corresponds to the turbine inlet temperature, which is limited to 200°C in order to ensure the feasibility of the direct-driven permanent-magnet generator. Indeed, high-power-density permanent magnets such as NdFeB are characterized by maximum operating temperatures around 240°C [74]. This temperature limitation also reduces the risk of thermal decomposition of the working fluid (except for R1233zd(E) as shown in Table 2). In terms of constraints, a minimum working fluid pressure of 1 bar is imposed in order to eliminate the risk of contamination by air and moisture, while a maximum pressure of 40 bar is considered for safety purpose [16]. For the sake of reliability, wet expansion is excluded in the turbines, while a minimum amount of subcooling is imposed at the inlet of the pumps in order to avoid cavitation. The subcooling is set such that the available net positive suction head (NPSH) at the pump inlet reaches 5% of the corresponding pump head. As a consequence, increased pressure rise over the pump leads to higher subcooling and higher condensation pressure. With regards to the pump and its motor efficiency, conservative assumptions are made. Finally, in order to guarantee a smooth operation of the engine WHR system independently of the season or geographic location, the ambient air temperature is fixed to 45°C. The remaining inputs in Table 3 are discussed in the later sections.

The thermodynamic cycle model is solved through the generic sequence presented in Figure 2. First (1), the condensation temperature/pressure is evaluated based on the condenser pinch input, while ensuring that the pressure is not lower than the minimum pressure constraint. Secondly (2), the evaporation pressures/temperatures are determined using the pressure ratio inputs, while ensuring that the maximum pressure constraint is not exceeded. Note that both sub- and super-critical "evaporations" are handled by the model. An iterative loop wraps steps 1-2 in order to obtain a subcooling that satisfies the pump NPSH constraint. Thirdly (3), the working fluid conditions are set at the outlet of the evaporators according to the evaporator pinch inputs, while ensuring that the maximum temperature input/constraint is also satisfied. For the SER1/2 configurations, this step concerns only the high-temperature evaporator. Then (4), the pump and turbine outlet conditions are

evaluated using the corresponding isentropic efficiencies, and (5) the regenerator outlet conditions are determined based on the regenerator pinch input. For the SER1/2 configurations, the working fluid conditions can now be evaluated at the outlet of the low-temperature evaporator. For the SER2 configuration, an additional iterative loop is implemented in order to determine the optimal intermediate temperature between the two regenerators (low-pressure side), while for the PAR2 configuration, such an iterative loop encompasses steps 4-5 in order to determine the optimal rotational speed of the two turbine stages. In a sixth step (6), the heat source outlet conditions are evaluated. Another iterative loop wraps steps 4-6 in order to find the working fluid mass flowrate satisfying the evaporator pinch inputs and the minimum heat source temperature constraints. Note that this loop is required because of the effect of mass flowrate on the turbine isentropic efficiency. Finally (7), the heat sink outlet conditions are evaluated based on the condenser pinch input and the maximum heat sink temperature constraint. Once the thermodynamic cycle is completed, the sizing of the heat exchangers and the preliminary design of the turbines and the rotor are performed.

Table 3: Model input variables, parameters and constraints

Variable	Range
(Low-pressure) Turbine pressure ratio	2 – 8
High-pressure turbine pressure ratio	2 – 8
Regenerator pinch	2 – 60 K
Condenser pinch	2 – 60 K
Low-temperature evaporator pinch	2 – 60 K
High-temperature evaporator pinch	2 – 60 K
Max. working fluid temperature	80 – 200°C
Parameter	**Assumption**
Ambient air temperature (at condenser inlet)	45°C
Mass flux in the inner tube of the heat exchangers	200 kg/(m^2s)
Mass flux in the outer tube of the heat exchangers	20 kg/(m^2s)
Exhaust gas fouling factor	0.002 K/W
Pump isentropic efficiency	60%
Motor mechanical efficiency	90%
Motor/Generator electrical efficiency	90%
Constraint	**Value**
Min. working fluid pressure	1 bar
Max. working fluid pressure	40 bar
Min. available NPSH at pump inlet	5% of total head
Min. vapor quality at turbine inlet/outlet	1
Max. air temperature lift	25 K
Min. exhaust gas temperature	150°C

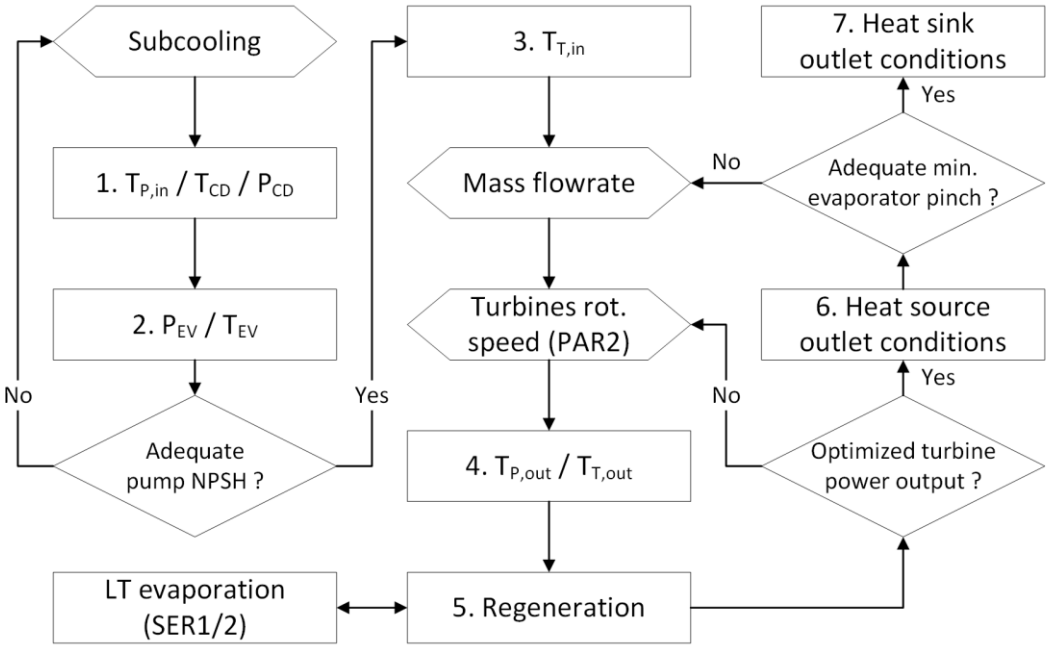

Figure 2: Generic solving procedure of the thermodynamic cycle

2.5 Heat exchanger model

In order to capture the effect of individual fluid properties when sizing the heat exchangers, a simple concentric-tube counter-flow design (Figure 3) is considered, where walls are assumed to be infinitely thin. The objective is to estimate the required heat exchange area based on the logarithmic mean temperature difference (LMTD) method [75] while using fluid-dependent overall heat transfer coefficients. Due to the higher pressure handling capability of smaller tubes, the highest-pressure fluid is always associated with the inner tube. Since heat source and sink fluids are assumed to be at 1 bar, they consequently always flow in the outer annular section of the heat exchangers. Similarly, the low-pressure gas-phase working fluid flows in the outer annulus of the regenerator. Since all the heat exchangers may involve two-phase flow on the high-pressure side, a generic 3-zone model is implemented, capable of handling subcooled, two-phase and superheated working fluid in the inner tube. The heat exchanger sizing procedure starts by determining tube diameters based on the mass flowrates and the imposed mass fluxes (see Table 3). At this point, average fluid properties (i.e. density, viscosity and thermal conductivity) are used together with tube diameters and resulting flow velocities, in order to determine inner and outer Reynolds numbers, friction factors, Nusselt numbers, and heat transfer coefficients $U_{i/o}$ in each zone. For this purpose, correlations for single-phase fully-developed flow through smooth circular and annular ducts are applied [76]. In the two-phase zone, the inner heat transfer coefficient is assumed to have a negligible effect on the overall heat transfer coefficient U (Equation 1). This assumption is justified by the much higher heat transfer coefficients typically obtained when condensing [77] or evaporating [78] a fluid in a circular tube compared to heating or cooling the same fluid in its single liquid/gas phase. However, high two-phase heat transfer coefficients are primarily obtained in the annular flow regime, which takes place at mass fluxes higher than 200 kg/(m^{2}s) [79]. This value has consequently been chosen for the sizing of the inner tubes. As for the outer tubes, a ten times smaller mass flux was imposed, which is equivalent to an air or exhaust gas flow velocity on the order of 20 m/s. This seems reasonable for achieving low pressure drops, and also considering the vehicle speed (33 m/s). Furthermore, since exhaust gases are expected to induce fouling in the high-temperature evaporator, an outer fouling factor F_o of 0.002 K/W [75] is considered in this case. Fouling is otherwise neglected. From the boundary temperature levels of each zone, the logarithmic mean temperature difference ΔT_{lm} can be computed (Equation 2) and the

corresponding heat exchange area A can finally be determined from Equation 3, where $\dot{Q}$ is the zone heat rate.

$$\frac{1}{U} = \frac{1}{U_i} + F_o + \frac{1}{U_o} \tag{1}$$

$$\Delta T_{lm} = \frac{|T_{i1} - T_{o2}| - |T_{i2} - T_{o1}|}{\ln(|T_{i1} - T_{o2}|/|T_{i2} - T_{o1}|)} \tag{2}$$

$$\dot{Q} = UA\Delta T_{lm} \tag{3}$$

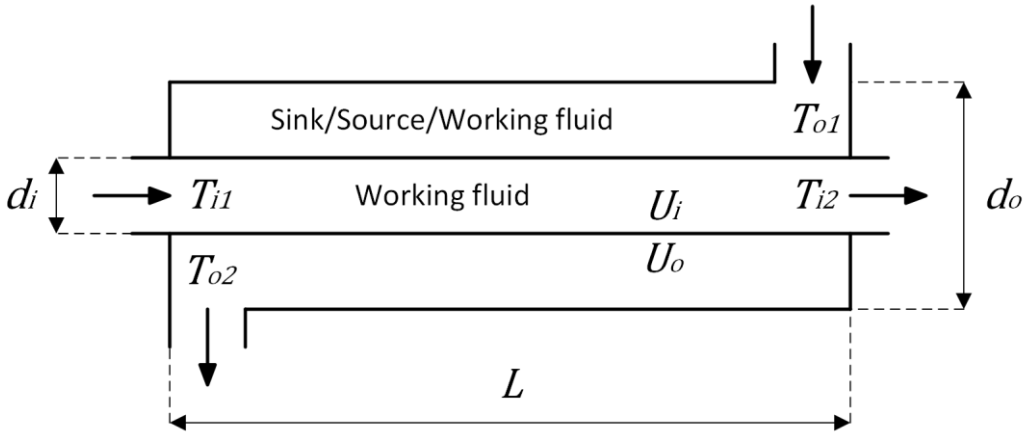

Figure 3: Concentric-tube counter-flow heat exchanger model

2.6 Turbomachinery model

Conventional preliminary design methodologies for turbines are based on similarity concepts introduced by Balje [80], where the turbine isentropic efficiency is given as a function of a specific speed and a specific diameter. However, Balje's diagrams were developed for large-scale turbines operated in sonic conditions and with low-density gases. They are consequently not suitable for designing small-scale ORC turbines. Instead, the pre-design maps proposed by Mounier et al. [81] for small-scale ORC radial-inflow turbines are used (Figure 4a). These maps were developed by fitting efficiency contours obtained from Monte Carlo simulations using an experimentally-validated 1D mean-line model [53] for such turbines. Beyond accounting for reduced scale and dense organic vapors, these maps introduce the turbine pressure ratio as an additional non-dimensional variable. Hence, with this model, the phenomenon of decreasing isentropic efficiency with increasing pressure ratio is well captured, as shown in Figure 4b. Although the map has been generated for pressure ratios up to 8, it should be noted that the original mean-line model tends to underestimate the isentropic efficiency for pressure ratios higher than 4.2, and so does the fitted model. Finally, the fitted model is convenient for optimization purpose, as it reduces the computation time by several orders of magnitude compared to the mean-line model. For most of the cycle configurations, the optimal isentropic efficiency associated with the considered pressure ratio is directly selected, together with the corresponding specific speed and diameter. For the dual-source dual-pressure configuration (PAR2), however, both turbines are constrained to the same rotational speed and their specific speeds and diameters are determined so that the total mechanical power output is maximized, even though their individual efficiencies may become suboptimal. Once the optimal specific speed and diameter have been determined, the turbine angular speed ω, tip diameter d_T, and tip speed u_T can be computed. The turbine tip speed is an indicator of the centrifugal stress level to which the turbine is exposed [82] and allows to draw conclusions with regards to the material selection.

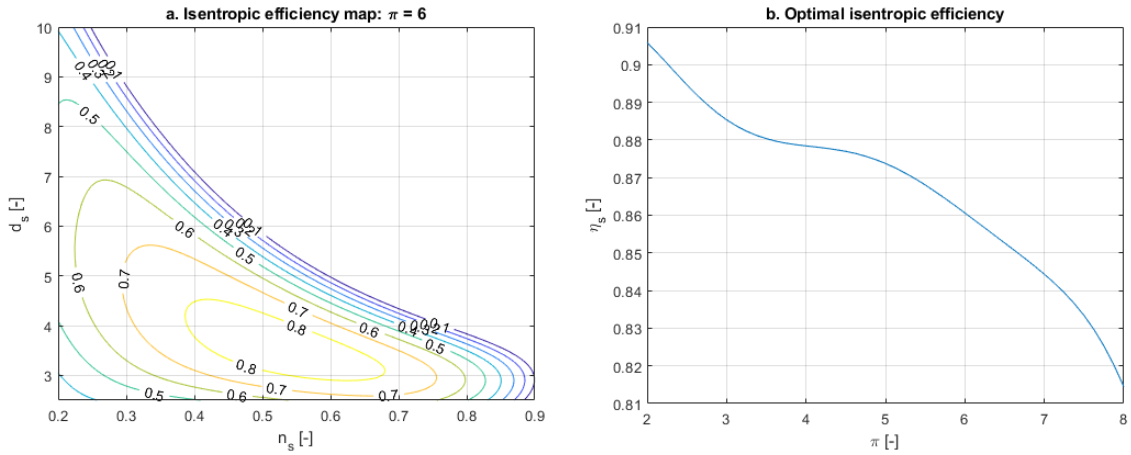

Figure 4: (a) Pre-design map example for a given pressure ratio
(b) Maximum efficiency as a function of the pressure ratio

2.7 Rotor model

The preliminary design of the rotor is shown schematically in Figure 5. It consists of a shaft supported on two journal bearings and a double-acting thrust bearing that are lubricated with the working fluid, and in which a cylindrical permanent magnet is fitted. Similarly to the heat exchangers, the goal is not to provide a detailed generator design but rather to introduce fluid- and speed-dependent mechanical losses in view of offering further insights into the effect of the working fluid selection for the turbo-ORC waste heat recovery system. As a consequence, fixed dimensional ratios (Table 4) based on the optimized geometries of gas bearings [83,84] and of high-speed permanent-magnet motors [85], are used. Note that the journal bearings diameter and inner thrust bearing diameter correspond to the shaft outer diameter. The magnet volume is determined from the output equation [86] (Equation 4), which expresses the magnetic torque τ_m as a function of the magnet volume V_m and the air-gap shear stress σ_g. For totally enclosed permanent-magnet machines, the air-gap shear stress may reach 21 N/m^2 [86], and this value is therefore applied for the sizing. Since the magnetic torque is initially unknown, an iterative loop is implemented in order to obtain a coherent torque value that includes the turbine work and the mechanical losses, which are dependent on the rotor design. The mechanical losses account for the journal bearings (Equation 5), thrust bearing (Equation 6) and generator windage (Equation 7) losses. Gas bearing losses result from viscous friction under laminar flow conditions and are derived by assuming a linear velocity profile across the bearing clearance. Generator windage losses arise from the growth of Taylor vortices in the air gap of the electrical machine. Vrancik [87] investigated these losses experimentally and derived an empirical correlation for the friction coefficient C_f (Equation 8), which is recommended for permanent-magnet machines [86]. The fluid density ρ and viscosity μ appearing in the mechanical loss equations are calculated by assuming that the fluid conditions in the generator are identical to the fluid conditions at the outlet of the (low-pressure) turbine. Although electrical losses are partially speed-dependent, numerous design options (topology and materials) are available for the stator of a permanent-magnet machine [86], thus allowing to mitigate the losses under the required operating conditions. A fixed conservative electrical efficiency is therefore assumed (see Table 3).

Table 4: Rotor design parameters

Design parameter	Algebraic expression	Value
Air-gap shear stress	σ_g	21 N/m^2
Ratio of magnet length to magnet radius	l_m/r_m	8.8
Ratio of rotor thickness to magnet radius	t_r/r_m	0.15
Ratio of air-gap clearance to rotor radius	c_g/r_r	0.1

Design parameter	Algebraic expression	Value
Ratio of coil width to magnet length	w_c/l_m	0.2
Ratio of radial bearing length to rotor radius	l_b/r_r	2
Ratio of axial bearing area to turbine front area	$(r_a^2 - r_r^2)/r_T^2$	1
Ratio of radial bearing clearance to rotor radius	c_b/r_r	0.001
Ratio of axial to radial bearing clearance	c_a/c_b	1

$$\tau_m = 2\sigma_g V_m = 2\sigma_g \pi r_m^2 l_m \tag{4}$$

$$\dot{Q}_b = 2 * 2\pi\mu\omega^2 \frac{r_r^3 l_b}{c_b} \tag{5}$$

$$\dot{Q}_a = 2 * \frac{\pi}{2}\mu\omega^2 \frac{r_a^4 - r_r^4}{c_a} \tag{6}$$

$$\dot{Q}_w = C_f \pi \rho \omega^3 r_r^4 (l_m + 2w_c) \tag{7}$$

$$\frac{1}{\sqrt{C_f}} = 2.04 + 1.768\, ln\left(\frac{\rho\omega r_r c_g}{\mu}\sqrt{C_f}\right) \tag{8}$$

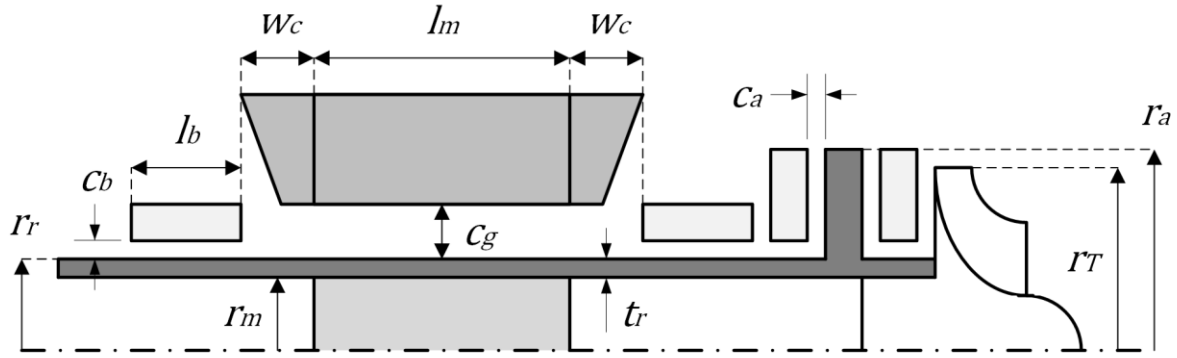

Figure 5: Schematic representation of the rotor concept

2.8 Optimization strategy

In order to identify the tradeoffs in terms of cycle configuration and working fluid for the proposed turbo-ORC system, an optimization is performed for each configuration-fluid pair, using Borg, an auto-adaptive multi-objective evolutionary algorithm [88]. Evolutionary algorithms are convenient when dealing with multi-input, non-linear and non-differentiable functions. Considering the passenger car application, the most appropriate objective functions are the system net power output (NPO) and total heat exchange area (HXA). Indeed, the first objective is a direct improvement of the vehicle efficiency and a measure of the potential for reducing fuel consumption and CO_2 emissions. As for the second objective, it allows comparing the required space in the vehicle from one solution to the other. Moreover, the heat exchange area is often used as a key indicator for the ORC system costs [56-58]. Finally, heat exchange areas can be used together with the typical surface area densities of suitable heat exchanger types, in order to provide rough volume estimates.

3. Results and discussion

3.1 Pareto fronts

The optimization results are presented in the Pareto fronts of Figure 6, showing the set of tradeoffs between the two objective functions for the investigated configurations and fluids. A maximum of 45'000 evaluations per optimization were necessary in order to achieve convergence. The results reveal that a maximum of 3 kW of electrical power could be produced by the WHR ORC system, corresponding to a 13.1% improvement in the engine power output under steady-state operating conditions of the passenger car on highway. This power boost, however, would be at the expense of 93 m^2 heat exchange area. With the same cycle configuration and working fluid, namely PAR2 and pentane, a reduction of the system net power output to 2 kW (-33%) would result in a 77% drop in the required heat exchange area. Similar tradeoffs are observed for all the studied configurations and fluids. Therefore, the set of Pareto fronts presented in Figure 6 is useful for determining the achievable engine efficiency improvement based on the available space in the vehicle. This confirms the importance of performing an integrated multi-objective optimization of the ORC system for such mobile applications.

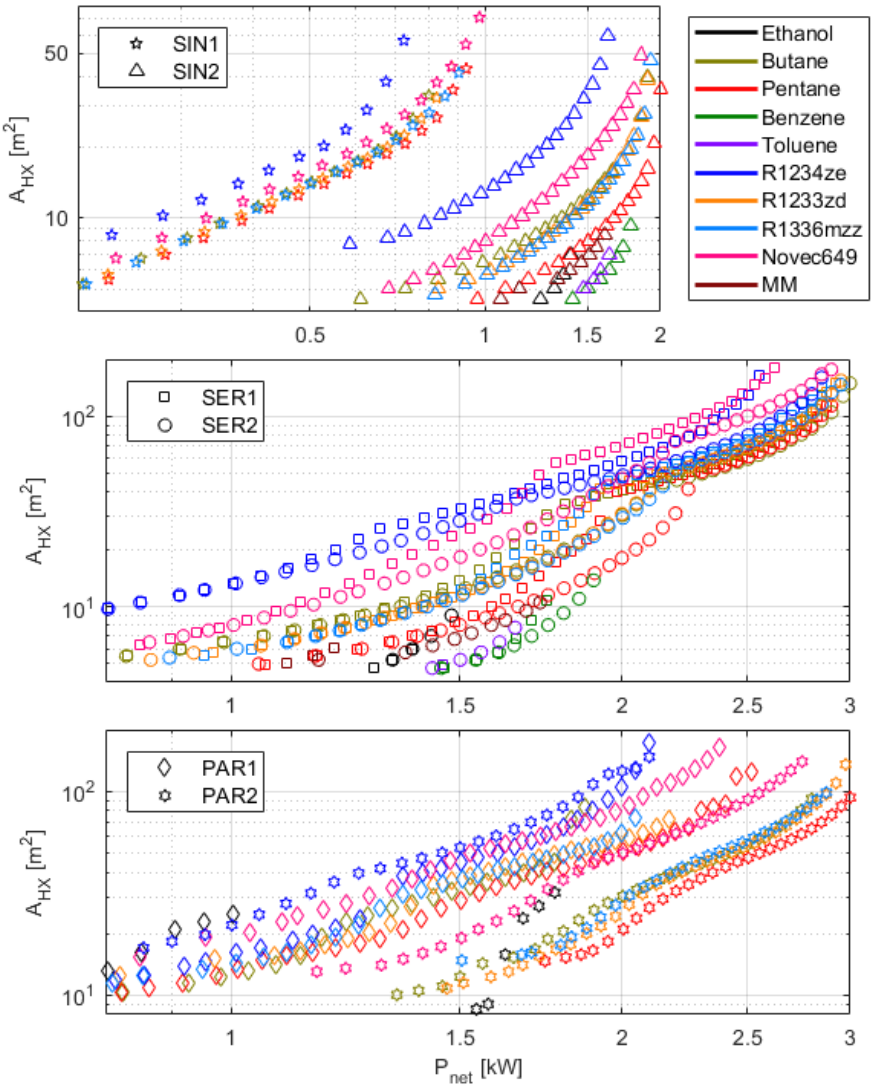

Figure 6: Pareto fronts for each pair of cycle configuration and working fluid

3.2 Configuration and fluid tradeoffs

In order to gain more insights into the WHR ORC system tradeoff mechanisms, the individual Pareto fronts of each cycle configuration and working fluid are investigated (Figure 7). Considering first the Pareto fronts according to the individual cycle configurations (Figure 7a), it is observed that the dual-pressure configuration (PAR2) outperforms the other ones at high NPO/HXA (> 2.2 kW and 30 m^2). The dual-regeneration configuration (SER2) is able to achieve as high NPO as the PAR2 configuration (up to 3 kW), however with significantly higher HXA. Yet, the SER2 configuration proves optimal at intermediate NPO/HXA, where it also provides a significant improvement compared to the single-regeneration dual-source configuration (SER1). Below 1.8 kW and 10 m^2, recovering energy from the engine coolant is not profitable anymore and the exhaust-gas-driven configuration (SIN2) performs similarly to the dual-source configurations with series evaporators. Among dual-source configurations with parallel evaporators, the single-pressure one (PAR1) considerably outperforms the dual-pressure one. Finally, the coolant-driven configuration (SIN1) presents the poorest performances and is only optimal at very low NPO (< 200 W). The lower performance of the PAR1 and SIN1 configurations results from the limited evaporation temperature permitted by the engine coolant.

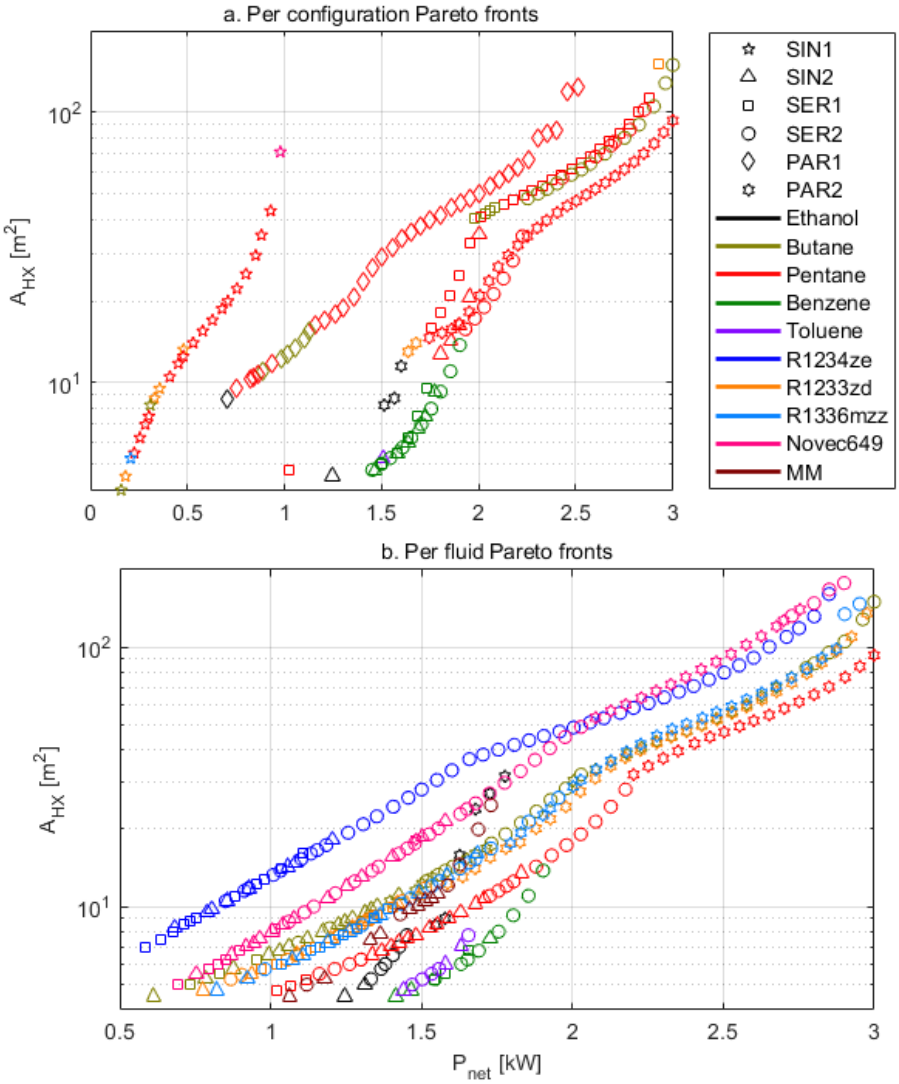

Figure 7: Individual Pareto fronts according to the cycle configurations (a) and the working fluids (b)

As shown in Figure 8, the condenser area represents the largest fraction (60-90%) of the HXA for all the cycles and independently of the NPO. It is consequently the most critical component for the

system integration in the vehicle. On the contrary, the high-temperature evaporator tends to have a minor area contribution, especially in the high-NPO regions. This is caused by (1) an inherently large logarithmic mean temperature difference between the exhaust gases and the working fluid, and (2) the higher turbine pressure ratios and lower condenser pinches characterizing the system in the high-NPO regions. The consequence is that the exhaust gas evaporator does not need to be large, or alternatively it can be designed larger than necessary in order to reduce the exhaust gas backpressure. On the other hand, a large condenser pinch causes the condensation temperature to increase, thus limiting the heat recovery potential from the engine coolant. This explains the null contribution of the low-temperature evaporator to the HXA in the low-NPO regions of dual-source configurations. Finally, the maximum contribution of the regenerator(s) to the HXA is obtained in the low-NPO region of the SER2 configuration. The sudden drop in the regenerator area and the resulting increase in the low-temperature evaporator area towards larger NPO is due to the transition to a lower turbine pressure ratio in which the coolant is used to evaporate the working fluid instead of only preheating it.

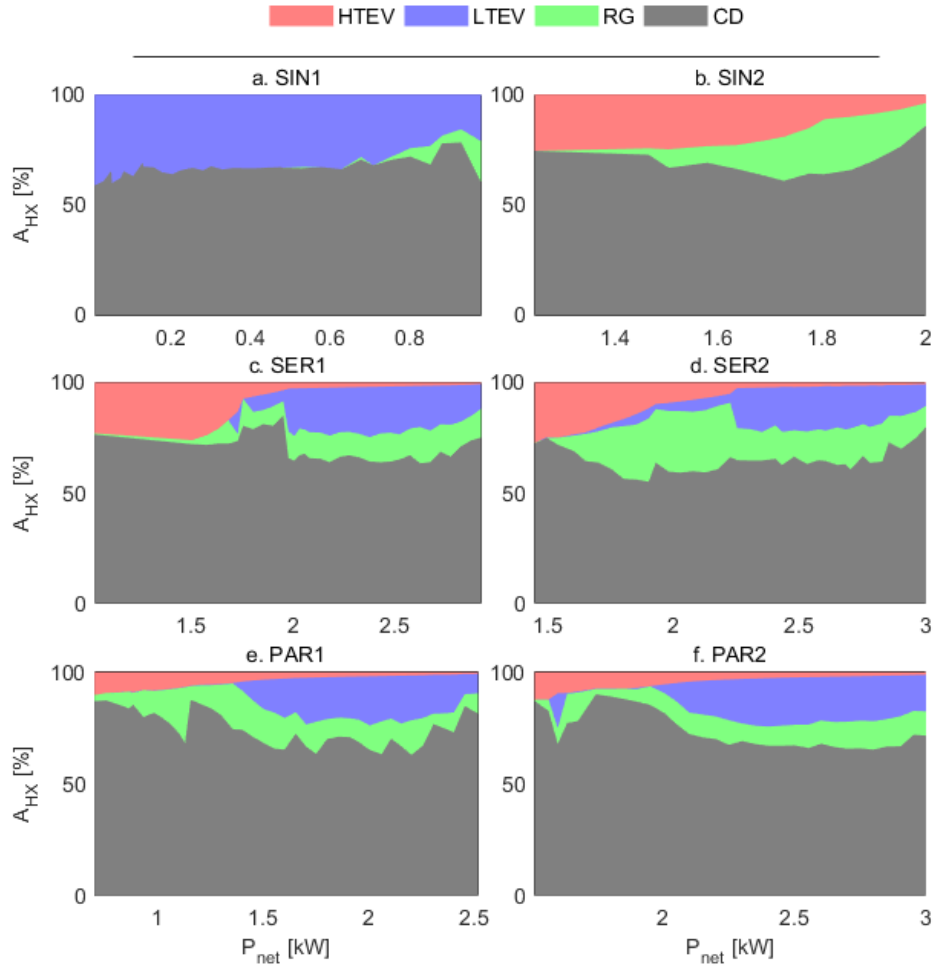

Figure 8: Heat exchanger area breakdown
along the Pareto front for each cycle configuration

In terms of working fluids, pentane is suggested to dominate the other investigated fluid, in particular in the high-HXA regions (Figure 7a). As shown in Figure 7b, benzene and toluene are also good candidates with intermediate NPO but relatively high specific power (in kW/m^2). Butane, R1233zd and R1336mzz compete with pentane but with substantially higher HXA for the same NPO. On the contrary, R1234ze and Novec649 are suboptimal fluids. The low performance of R1234ze is explained by its low boiling point, which implies high and even supercritical operating pressures (Figure 9c), resulting in limited turbine pressure ratios (due to the maximum pressure constraint) and significant cycle backwork ratios (Figure 9d). Butane also suffers from this drawback but to a lesser extent. Conversely, ethanol, benzene, toluene and MM are characterized by high boiling points,

resulting in low reduced evaporation pressures and low cycle backwork ratios. However, their inherent drawback is the condensation at sub-atmospheric pressures. Since, the minimum condensation pressure has been constrained to 1 bar, their performance is consequently limited. Based on these observations, the optimum working fluids should have a boiling point close to the heat sink temperature and a high critical pressure. Yet, these conditions are not sufficient, as observed with the low performance of Novec649. Indeed, the hydrofluoroketone features a very low turbine power output compared to the cycle heat input (Figure 9b). The investigated siloxane (MM) is also characterized by a limited relative turbine power output compared to hydrocarbons and hydrofluorocarbons, thus suggesting that these fluids are more suitable for the considered application. In terms of temperature, all the optimum system designs tend to converge to the maximum allowed temperature (Figure 9a), suggesting that higher system NPO could be reached with higher operating temperatures. However, as discussed in section 2.4, the thermal management of a direct-driven permanent-magnet generator with a turbine inlet temperature higher than 200°C would be challenging.

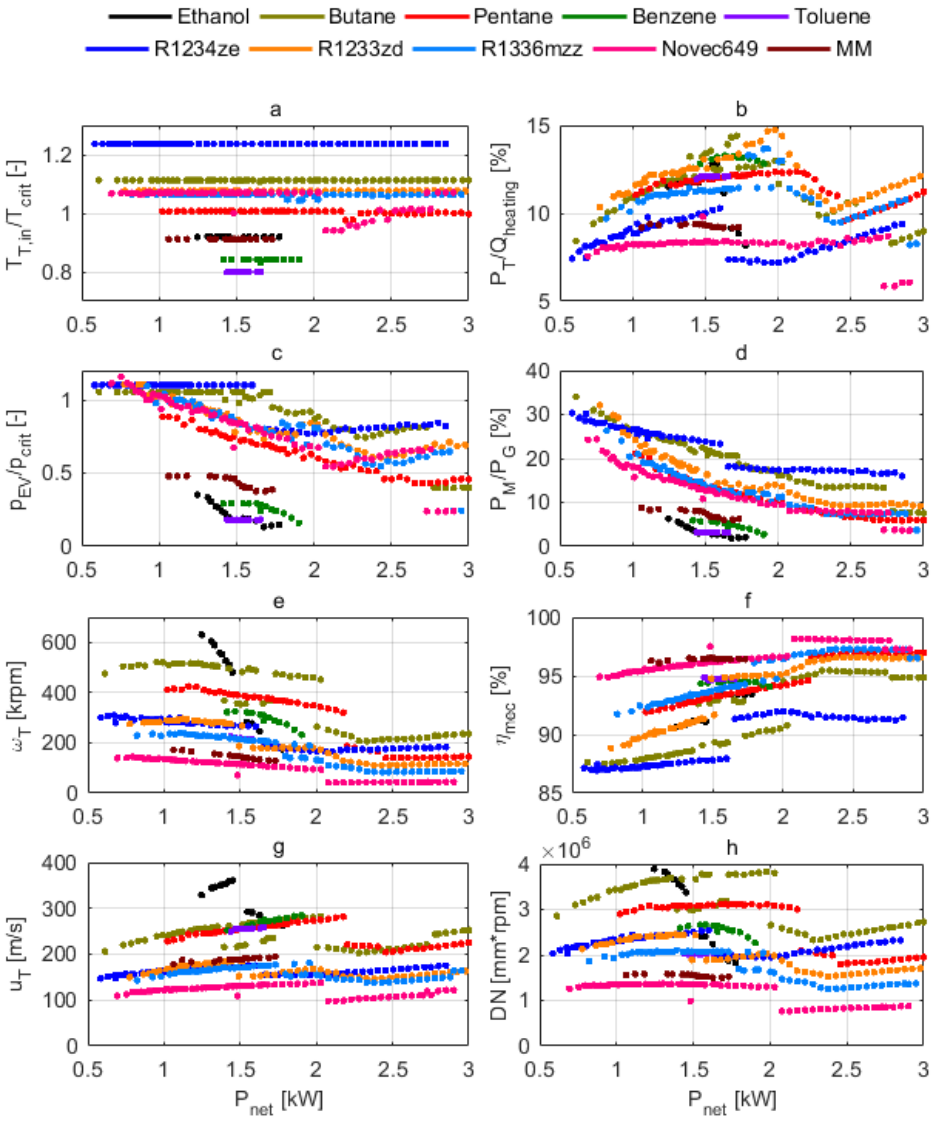

Figure 9: Performance indicators and operating conditions along the Pareto front for each working fluid

With regards to the optimal turbine design, the investigated alcohol (ethanol) and hydrocarbons require much higher rotational speeds (Figure 9e) and more challenging tip speeds (Figure 9g) compared to the other working fluids. This is a direct consequence of their lower molecular weights.

Higher rotor speeds also result in higher mechanical losses (Figure 9f), causing additional heat generation in the vicinity of the generator magnet, which is to be avoided. Finally, higher speeds increase the DN number of the radial bearings (Figure 9h). Ethanol, butane and pentane feature challenging DN numbers for self-acting gas bearings (> $3 \cdot 10^6$) [89]. Note that the dual-pressure cycle configuration considerably mitigates the required turbine rotational speeds, tip speeds and bearing DN numbers, also increasing the rotor mechanical efficiency.

3.3 Constrained overall Pareto fronts

In order to determine the optimal system design, the cycle configuration and the working fluid can be picked on the overall Pareto front based on the heat exchanger area that can be fitted in the vehicle. However, the corresponding system characteristics may not be optimal from the operational point of view. On the one hand, the turbine tip speed may be too high for the turbine to be manufactured out of a conventional material, or the bearing DN number may be challenging for self-acting gas bearings. On the other hand, a flammable fluid may not be allowed for the passenger car application. As a consequence, two overall Pareto fronts (Figure 10a) are extracted from the optimization results, one for the flammable fluids (hydrocarbons) and one for the low-flammability fluids (hydrofluorocarbons), while both of them are constrained to solutions with a bearing DN number lower than $3 \cdot 10^6$. The split of the overall heat exchange area is presented in Figure 10b/c, once again suggesting a dominance of the condenser area.

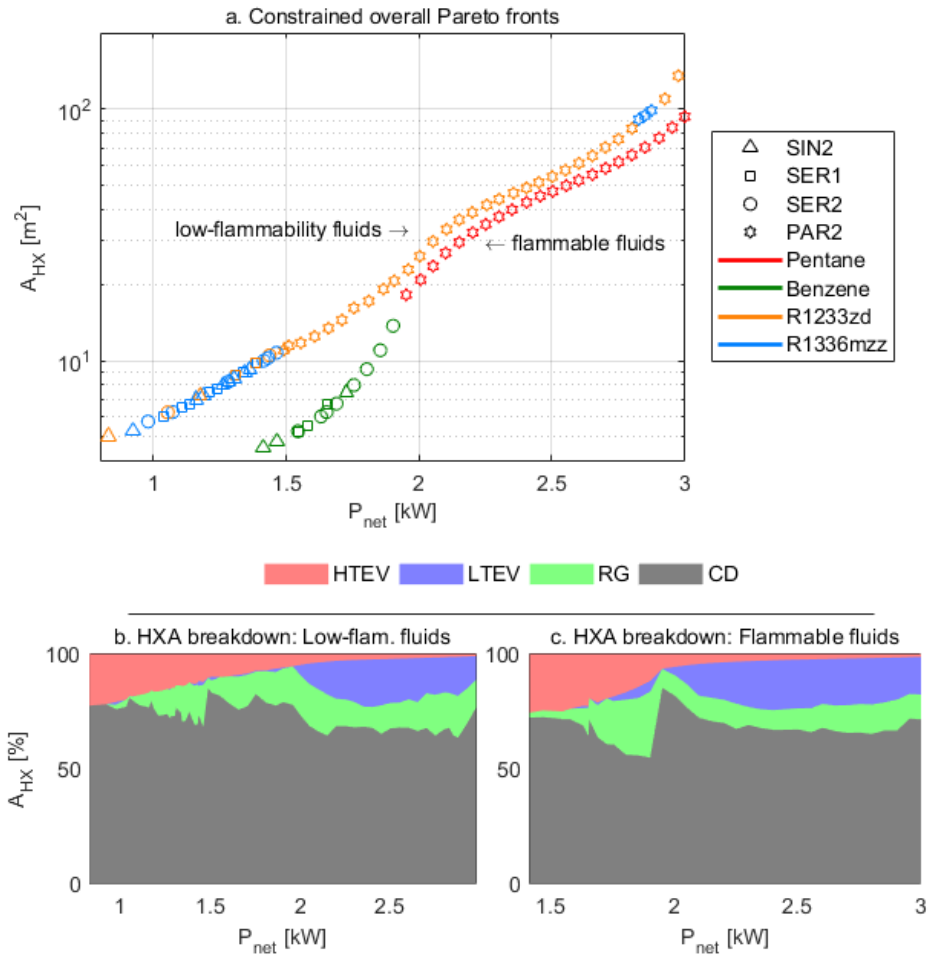

Figure 10: Constrained overall Pareto fronts
and corresponding heat exchanger area breakdowns

In terms of operating conditions, the flammable fluids present lower pressure levels (Figure 11a/b) and lower cycle backwork ratios (Figure 11c), while the low-flammability fluids are characterized by

lower turbine rotational speeds (Figure 11e), and convenient turbine tip speeds (Figure 11f). The high-NPO region of the Pareto fronts is dominated by the dual-pressure cycle configuration for both fluid categories. This configuration provides a number of advantages including lower pressure levels, lower speeds, and higher mechanical efficiencies, up to 97% (Figure 11g). The optimal turbine rotational speeds (Figure 11e) range from 80 to 290 krpm for low-flammability fluids and from 140 to 330 krpm for flammable fluids, while the optimal turbine tip diameters (Figure 11d) are similar for both fluid categories, ranging from 10 to 33 mm for the low-pressure turbine and from 13 to 23 mm for the high-pressure turbine. Due to the higher mass flowrate across the low-pressure turbine (especially at high system NPO), the internal optimization loop included in the dual-pressure cycle configuration model tends to maximize the isentropic efficiency of the low-pressure stage at the expense of a lower efficiency for the high-pressure stage (Figure 11h).

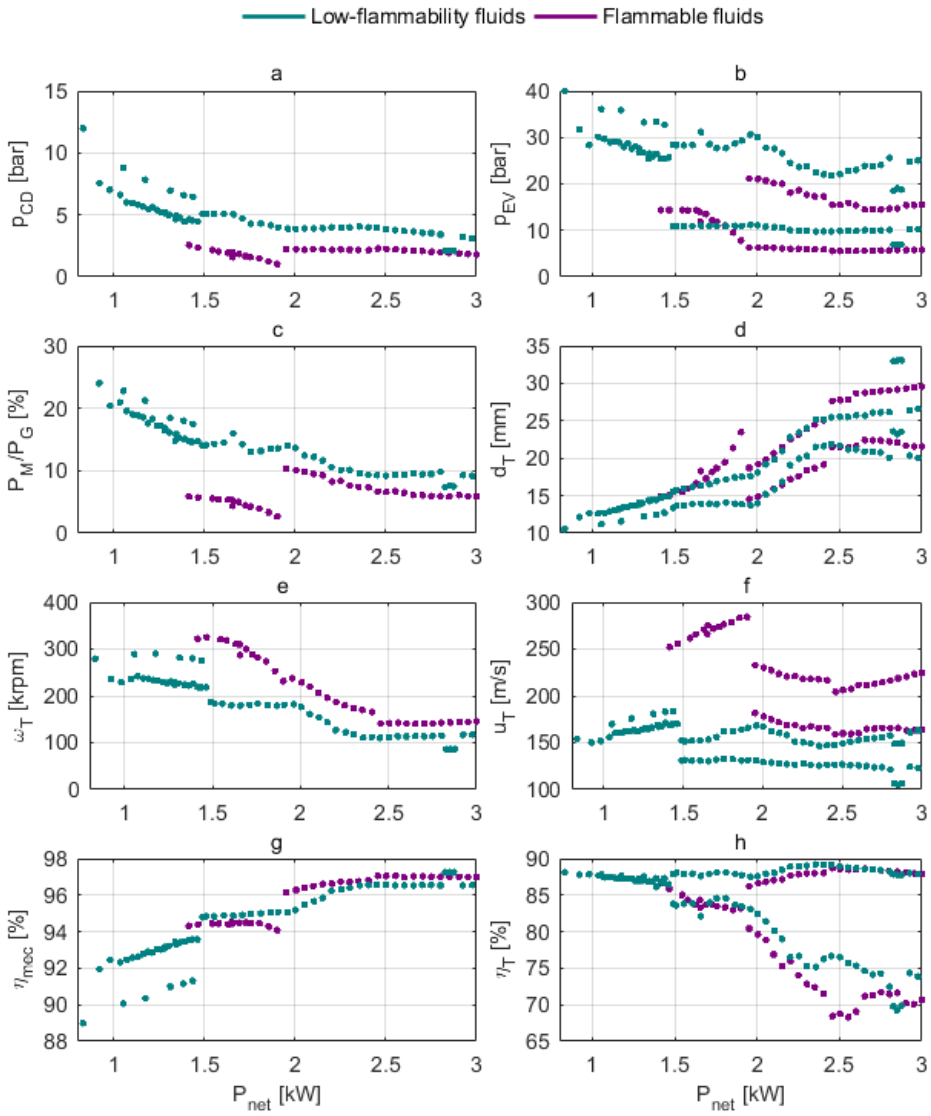

Figure 11: Performance indicators and operating conditions along the constrained overall Pareto fronts

3.4 Application example

According to Shah and Sekulic [90], the surface area density of a plate-fin flat-tube heat exchanger with 600 fins/m is about 1300 m^2/m^3, while reaching 720 m^2/m^3 for a shell-and-finned-tube heat exchanger with 400 fins/m. As discussed in section 1, such heat exchangers are both suitable for mobile ORC condenser and evaporator. For the regenerator, plate heat exchangers with surface area

densities up to 660 m^2/m^3 [90] may be suitable. Since the condenser is the major contributor to the system heat exchange area, it is assumed that an average surface area density of 1000 m^2/m^3 is achievable for an on-board ORC system. Figure 12 presents the Ts diagrams of the optimal cycles for 0.01 and 0.04 m^3 of heat exchanger volume, which seem a reasonable range in view of the size of an average passenger car. The optimal working fluids are all isentropic-dry and regeneration is significant in all cases, which confirms the importance of integrating a regenerator in the system. In addition to improving the cycle efficiency, the regenerator reduces the amount of heat to be evacuated by the condenser, therefore reducing the condenser area. The low-HXA systems (Figure 12a/b) are characterized by a large pinch in the condenser, thus leading to higher condensation and evaporation temperatures. As a consequence, the engine coolant is used only to preheat the liquid-phase working fluid. However, the available waste heat in the coolant is partially recovered. This explains why the exhaust-gas-driven (single-source) configuration performs as good as the dual-source series-evaporator configurations at low NPO. Conversely, the optimal dual-source dual-pressure configurations (Figure 12c/d) are ideal for maximizing the waste heat recovery from both the engine coolant and exhaust gases.

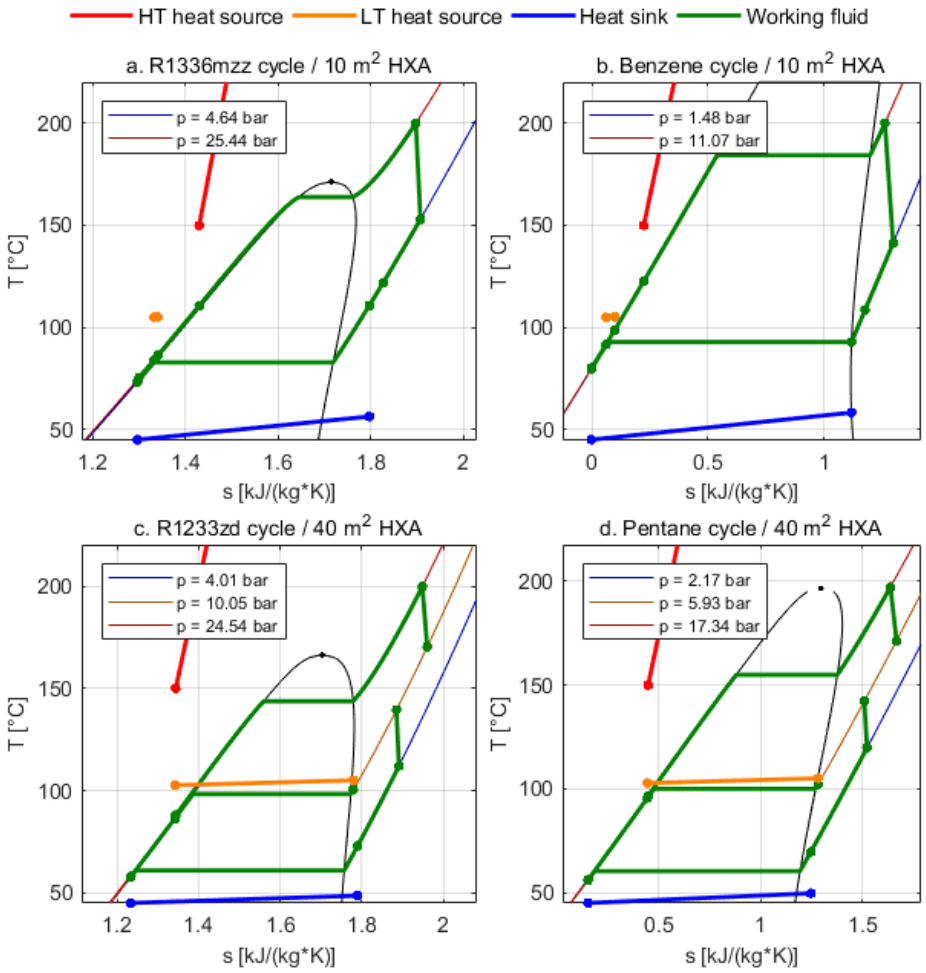

Figure 12: Ts diagrams of the optimal cycles for 10 m^2 (a/b) and 40 m^2 (c/d) of heat exchange area

4. Conclusions and outlook

Different organic Rankine cycle configurations operated with various working fluids have been compared in view of their application to passenger car waste heat recovery, considering both engine coolant and exhaust gases as heat source. Due to their high-power density and high expansion ratio capability, radial-inflow turbines were considered as the expansion device. The corresponding isentropic efficiencies were evaluated based on an updated preliminary design map accounting for the effect of the pressure ratio. The turbine was assumed to be directly coupled to a permanent-magnet

generator, using gas bearings lubricated with the working fluid to support the high-speed rotor. A preliminary design of the rotor allowed estimating the fluid- and speed-dependent mechanical losses. A constrained multi-variable and multi-objective optimization of the system net power output and heat exchange area was performed, using an evolutionary algorithm. The results of this procedure suggest that:

- The multi-objective optimization of ORC systems for passenger car engine WHR, focusing not only on the thermodynamic performance but also on the system size, is essential in order to determine the achievable engine efficiency improvement based on the available space in the vehicle.
- The optimal cycle configuration and working fluid depend on the amount of heat exchange area that can be fitted in the vehicle. Below a certain threshold, recovering energy from the engine coolant is not profitable and the exhaust-gas-driven cycle configuration is preferable. Above this threshold, the dual-source dual-pressure cycle configuration is optimal.
- Independently of the configuration, fluid and net power output, the condenser represents 60-90% of the required heat exchange area and is consequently the most critical component for the system integration in the vehicle.
- Regeneration is an essential mechanism that allows both improving the cycle efficiency and reducing the amount of heat to be evacuated by the condenser, therefore reducing its area.
- The dual-source dual-regeneration and dual-source dual-pressure cycle configurations provide the highest system net power output (up to 3 kW), corresponding to a 13% peak improvement in the engine power output under steady-state operating conditions. The former one includes an additional heat exchanger and is typically characterized by a higher heat exchange area. The latter one involves two turbine stages and is consequently more complex.
- Hydrocarbons and hydrofluorocarbons, especially pentane and R1233zd(E), are the most suitable working fluid candidates for vehicle engine WHR ORC systems. For a given heat exchange area, hydrocarbons provide a higher system net power output compared to hydrofluorocarbons. In addition, they require lower operating pressures and allow for reduced cycle backwork ratios. However, they are flammable and imply higher turbine rotational speeds, leading to challenging turbine tip speeds and bearing DN numbers. Moreover, higher rotational speeds result in lower mechanical efficiencies, causing more heat generation in the vicinity of the generator magnet.
- The most suitable working fluids for high-temperature WHR applications are characterized by (1) a boiling point close to the heat sink temperature, (2) a high critical pressure, and (3) a high molecular weight. These criteria favor high system efficiency and low turbine rotational speed.
- The optimal turbine designs along the overall Pareto front feature rotational speeds ranging from 80 to 330 krpm and tip diameters ranging from 10 to 33 mm.

Supported on gas bearings and driving a permanent-magnet generator, radial-inflow turbines may consequently be suitable for ORC-based WHR from ICE-powered passenger car. Nevertheless, many challenging technological and operational aspects still need to be addressed. Efficient, compact, reliable and cost-effective components must be developed for this specific application, in particular the expander and the pump. Furthermore, system integration in the vehicle as well as optimal control under the inherently transient engine conditions need to be further investigated. Due to the severe cost and space constraints associated with passenger cars, mobile WHR ORC systems are more likely to penetrate the market within long-haul trucks. Future work will consequently focus on this application and in particular on the detailed design and performance assessment of a suitable ORC turbo-generator.

Nomenclature

Symbols

A	Area	m^2
c	Clearance	m
C_f	Friction coefficient	$-$
d	Diameter	m
d_s	Specific diameter	$-$
DN	Bearing DN number	$mm \cdot rpm$

$\dot{E}$	Exergy rate	W
F	Fouling factor	K/W
l	Length	m
m	Molecular weight	$kg/kmol$
$\dot{m}$	Mass flowrate	kg/s
n_s	Specific speed	$-$
P	Power	W
p	Pressure	bar
$\dot{Q}$	Heat rate	W
r	Radius	m
s	Entropy	$J/(kg \cdot K)$
T	Temperature	K
t	Thickness	m
U	Heat transfer coefficient	$W/(m^2 \cdot K)$
u	Tip speed	m/s
V	Volume	m^3
$\dot{V}$	Volumetric flowrate	m^3/s
w	Width	m
ΔT	Temperature difference	K
η	Efficiency	$-$
μ	Dynamic viscosity	$Pa \cdot s$
ξ	Slope of the saturated vapor curve	$J/(kg \cdot K^2)$
π	Pressure ratio	$-$
ρ	Density	kg/m^3
σ_g	Air-gap shear stress	Pa
τ	Torque	$N \cdot m$
ω	Angular speed	rad/s

Subscripts

a	Axial bearing
b	Radial bearing
$boil$	Boiling point
CD	Condensation
c	Coil
$crit$	Critical point
EV	Evaporation
eng	Engine
G	Generator
g	Air-gap
HX	Heat exchange
i	Inner
in	Inlet
lm	Logarithmic mean
M	Motor
m	Magnet(ic)
mec	Mechanical
o	Outer
r	Rotor
s	Isentropic
T	Turbine

Acronyms

CD	Condenser
GWP	Global warming potential
HC	Hydrocarbon
HCFO	Hydrochlorofluoroolefin
HFK	Hydrofluoroketone
HFO	Hydrofluoroolefin
HTEV	High-temperature evaporator
HXA	Heat exchange area
ICE	Internal combustion engine
LMTD	Logarithmic mean temperature difference
LTEV	Low-temperature evaporator
MM	Hexamethyldisiloxane
MPG	Mono propylene glycol
NPO	Net power output
NPSH	Net positive suction head
ODP	Ozone depletion potential
ORC	Organic Rankine cycle
PAR1	Dual-source cycle with parallel evaporators
PAR2	Dual-source dual-pressure cycle with parallel evaporators
RG	Regenerator
SER1	Dual-source cycle with series evaporators
SER2	Dual-source dual-regeneration cycle with series evaporators
SIN1	Single-source cycle using engine coolant
SIN2	Single-source cycle using engine exhaust gases
WHR	Waste heat recovery

References

[1] IEA. Key World Energy Statistics 2017 2017.
[2] IEA. CO2 Emissions From Fuel Combustion Highlights 2017 2017.
[3] ICCT. European vehicle market statistics 2015/16 2015.

[4] Thomas J. Drive Cycle Powertrain Efficiencies and Trends Derived from EPA Vehicle Dynamometer Results. SAE Int J Passeng Cars - Mech Syst 2014;7:1374–84. doi:10.4271/2014-01-2562.
[5] Atabani AE, Badruddin IA, Mekhilef S, Silitonga AS. A review on global fuel economy standards, labels and technologies in the transportation sector. Renewable and Sustainable Energy Reviews 2011;15:4586–610. doi:10.1016/j.rser.2011.07.092.
[6] THE EUROPEAN PARLIAMENT AND THE COUNCIL OF THE EUROPEAN UNION. REGULATION (EC) No 443/2009 OF THE EUROPEAN PARLIAMENT AND OF THE COUNCIL of 23 April 2009 setting emission performance standards for new passenger cars as part of the Community's integrated approach to reduce CO2 emissions from light-duty vehicles 2009.
[7] Freymann R, Strobl W, Obieglo A. The turbosteamer: A system introducing the principle of cogeneration in automotive applications. MTZ Worldw 2008;69:20–7. doi:10.1007/BF03226909.
[8] Sprouse III C, Depcik C. Review of organic Rankine cycles for internal combustion engine exhaust waste heat recovery. Applied Thermal Engineering 2013;51:711–22. doi:10.1016/j.applthermaleng.2012.10.017.
[9] Colonna P, Casati E, Trapp C, Mathijssen T, Larjola J, Turunen-Saaresti T, et al. Organic Rankine Cycle Power Systems: From the Concept to Current Technology, Applications, and an Outlook to the Future. J Eng Gas Turbines Power 2015;137:100801–100801. doi:10.1115/1.4029884.
[10] Dai Y, Wang J, Gao L. Parametric optimization and comparative study of organic Rankine cycle (ORC) for low grade waste heat recovery. Energy Conversion and Management 2009;50:576–82. doi:10.1016/j.enconman.2008.10.018.
[11] Wang EH, Zhang HG, Fan BY, Ouyang MG, Zhao Y, Mu QH. Study of working fluid selection of organic Rankine cycle (ORC) for engine waste heat recovery. Energy 2011;36:3406–18. doi:10.1016/j.energy.2011.03.041.
[12] Vaja I, Gambarotta A. Internal Combustion Engine (ICE) bottoming with Organic Rankine Cycles (ORCs). Energy 2010;35:1084–93. doi:10.1016/j.energy.2009.06.001.
[13] Boretti A. Recovery of exhaust and coolant heat with R245fa organic Rankine cycles in a hybrid passenger car with a naturally aspirated gasoline engine. Applied Thermal Engineering 2012;36:73–7. doi:10.1016/j.applthermaleng.2011.11.060.
[14] Katsanos CO, Hountalas DT, Pariotis EG. Thermodynamic analysis of a Rankine cycle applied on a diesel truck engine using steam and organic medium. Energy Conversion and Management 2012;60:68–76. doi:10.1016/j.enconman.2011.12.026.
[15] Grelet V, Reiche T, Lemort V, Nadri M, Dufour P. Transient performance evaluation of waste heat recovery rankine cycle based system for heavy duty trucks. Applied Energy 2016;165:878–92. doi:10.1016/j.apenergy.2015.11.004.
[16] Seher D, Lengenfelder T, Gerhardt J, Eisenmenger N, Hackner M, Krinn I. Waste heat recovery for commercial vehicles with a Rankine process, Aachen, Germany: 2012.
[17] Lang W, Colonna P, Almbauer R. Assessment of Waste Heat Recovery From a Heavy-Duty Truck Engine by Means of an ORC Turbogenerator. J Eng Gas Turbines Power 2013;135:042313–042313. doi:10.1115/1.4023123.
[18] Kim YM, Shin DG, Kim CG, Cho GB. Single-loop organic Rankine cycles for engine waste heat recovery using both low- and high-temperature heat sources. Energy 2016;96:482–94. doi:10.1016/j.energy.2015.12.092.
[19] Panesar AS. An innovative Organic Rankine Cycle system for integrated cooling and heat recovery. Applied Energy 2017;186:396–407. doi:10.1016/j.apenergy.2016.03.011.

[20] Chen T, Zhuge W, Zhang Y, Zhang L. A novel cascade organic Rankine cycle (ORC) system for waste heat recovery of truck diesel engines. Energy Conversion and Management 2017;138:210–23. doi:10.1016/j.enconman.2017.01.056.
[21] Wang EH, Zhang HG, Zhao Y, Fan BY, Wu YT, Mu QH. Performance analysis of a novel system combining a dual loop organic Rankine cycle (ORC) with a gasoline engine. Energy 2012;43:385–95. doi:10.1016/j.energy.2012.04.006.
[22] Shu G, Liu L, Tian H, Wei H, Xu X. Performance comparison and working fluid analysis of subcritical and transcritical dual-loop organic Rankine cycle (DORC) used in engine waste heat recovery. Energy Conversion and Management 2013;74:35–43. doi:10.1016/j.enconman.2013.04.037.
[23] Shu G, Liu L, Tian H, Wei H, Liang Y. Analysis of regenerative dual-loop organic Rankine cycles (DORCs) used in engine waste heat recovery. Energy Conversion and Management 2013;76:234–43. doi:10.1016/j.enconman.2013.07.036.
[24] Chen H, Goswami DY, Stefanakos EK. A review of thermodynamic cycles and working fluids for the conversion of low-grade heat. Renewable and Sustainable Energy Reviews 2010;14:3059–67. doi:10.1016/j.rser.2010.07.006.
[25] Juhasz JR, Simoni LD. A review of potential working fluids for low temperature organic Rankine cycles in waste heat recovery. Proceedings of the 3rd International Seminar on ORC Power Systems, Brussels, Belgium: University of Liège and Ghent University; 2015.
[26] Preissinger M, Brüggemann D. Thermal stability of hexamethyldisiloxane (MM) for high temperature applications. Proceedings of the 3rd International Seminar on ORC Power Systems, Brussels, Belgium: University of Liège and Ghent University; 2015.
[27] Pasetti M, Invernizzi CM, Iora P. Thermal stability of working fluids for organic Rankine cycles: An improved survey method and experimental results for cyclopentane, isopentane and n-butane. Applied Thermal Engineering 2014;73:764–74. doi:10.1016/j.applthermaleng.2014.08.017.
[28] Invernizzi CM, Iora P, Preißinger M, Manzolini G. HFOs as substitute for R-134a as working fluids in ORC power plants: A thermodynamic assessment and thermal stability analysis. Applied Thermal Engineering 2016;103:790–7. doi:10.1016/j.applthermaleng.2016.04.101.
[29] Invernizzi CM, Iora P, Manzolini G, Lasala S. Thermal stability of n-pentane, cyclo-pentane and toluene as working fluids in organic Rankine engines. Applied Thermal Engineering 2017;121:172–9. doi:10.1016/j.applthermaleng.2017.04.038.
[30] Erhart T, Gölz J, Eicker U, van den Broek M. Fluid stability in large scale ORCs using siloxanes - Long-term experiences and fluid recycling. Proceedings of the 3rd International Seminar on ORC Power Systems, Brussels, Belgium: University of Liège and Ghent University; 2015.
[31] Eyerer S, Eyerer P, Eicheldinger M, Sax S, Wieland C, Spliethoff H. Material compatibility of ORC working fluids with polymers. Energy Procedia 2017;129:137–44. doi:10.1016/j.egypro.2017.09.189.
[32] Imran M, Usman M, Park B-S, Lee D-H. Volumetric expanders for low grade heat and waste heat recovery applications. Renewable and Sustainable Energy Reviews 2016;57:1090–109. doi:10.1016/j.rser.2015.12.139.
[33] Wu Z, Pan D, Gao N, Zhu T, Xie F. Experimental testing and numerical simulation of scroll expander in a small scale organic Rankine cycle system. Applied Thermal Engineering 2015;87:529–37. doi:10.1016/j.applthermaleng.2015.05.040.
[34] Tang H, Wu H, Wang X, Xing Z. Performance study of a twin-screw expander used in a geothermal organic Rankine cycle power generator. Energy 2015;90:631–42. doi:10.1016/j.energy.2015.07.093.

[35] Galindo J, Ruiz S, Dolz V, Royo-Pascual L, Haller R, Nicolas B, et al. Experimental and thermodynamic analysis of a bottoming Organic Rankine Cycle (ORC) of gasoline engine using swash-plate expander. Energy Conversion and Management 2015;103:519–32. doi:10.1016/j.enconman.2015.06.085.
[36] Cipollone R, Bianchi G, Di Battista D, Contaldi G, Murgia S. Mechanical Energy Recovery from Low Grade Thermal Energy Sources. Energy Procedia 2014;45:121–30. doi:10.1016/j.egypro.2014.01.014.
[37] Cipollone R, Bianchi G, Gualtieri A, Battista DD, Mauriello M, Fabio Fatigati. Development of an Organic Rankine Cycle system for exhaust energy recovery in internal combustion engines. J Phys: Conf Ser 2015;655:012015. doi:10.1088/1742-6596/655/1/012015.
[38] Di Battista D, Mauriello M, Cipollone R. Waste heat recovery of an ORC-based power unit in a turbocharged diesel engine propelling a light duty vehicle. Applied Energy 2015;152:109–20. doi:10.1016/j.apenergy.2015.04.088.
[39] Olmedo LE, Mounier V, Mendoza LC, Schiffmann J. Dimensionless correlations and performance maps of scroll expanders for micro-scale Organic Rankine Cycles. Energy 2018. doi:10.1016/j.energy.2018.05.001.
[40] Youbi-Idrissi M, Bonjour J. The effect of oil in refrigeration: Current research issues and critical review of thermodynamic aspects. International Journal of Refrigeration 2008;31:165–79. doi:10.1016/j.ijrefrig.2007.09.006.
[41] Bao J, Zhao L. A review of working fluid and expander selections for organic Rankine cycle. Renewable and Sustainable Energy Reviews 2013;24:325–42. doi:10.1016/j.rser.2013.03.040.
[42] Rosset K, Mounier V, Guenat E, Pajot O, Schiffmann J. Potential of small-scale turbomachinery for waste heat recovery on automotive internal combustion engines. Proceedings of the 3rd International Seminar on ORC Power Systems, Brussels, Belgium: University of Liège and Ghent University; 2015.
[43] Mounier V, Mendoza LC, Schiffmann J. Thermo-economic optimization of an ORC driven heat pump based on small scale turbomachinery and comparison with absorption heat pumps. International Journal of Refrigeration 2017;81:96–110. doi:10.1016/j.ijrefrig.2017.05.021.
[44] Freymann R, Ringler J, Seifert M, Horst T. The Second Generation Turbosteamer. MTZ Worldw 2012;73:18–23. doi:10.1365/s38313-012-0138-1.
[45] Seume JR, Peters M, Kunte H. Design and test of a 10kW ORC supersonic turbine generator. J Phys: Conf Ser 2017;821:012023. doi:10.1088/1742-6596/821/1/012023.
[46] Battista DD, Cipollone R. Experimental Analysis of an Organic Rankine Cycle Plant Bottoming a Heavy-Duty Engine Using Axial Turbine as Prime Mover. SAE Int J Engines 2017;10:1385–97. doi:10.4271/2017-01-9279.
[47] Pini M, De Servi C, Burigana M, Bahamonde S, Rubino A, Vitale S, et al. Fluid-dynamic design and characterization of a mini-ORC turbine for laboratory experiments. Energy Procedia 2017;129:1141–8. doi:10.1016/j.egypro.2017.09.186.
[48] Alshammari F, Pesyridis A, Karvountzis-Kontakiotis A, Franchetti B, Pesmazoglou Y. Experimental study of a small scale organic Rankine cycle waste heat recovery system for a heavy duty diesel engine with focus on the radial inflow turbine expander performance. Applied Energy 2018;215:543–55. doi:10.1016/j.apenergy.2018.01.049.
[49] Guillaume L, Legros A, Desideri A, Lemort V. Performance of a radial-inflow turbine integrated in an ORC system and designed for a WHR on truck application: An experimental comparison between R245fa and R1233zd. Applied Energy 2017;186, Part 3:408–22. doi:10.1016/j.apenergy.2016.03.012.

[50] Schiffmann J, Favrat D. Experimental investigation of a direct driven radial compressor for domestic heat pumps. International Journal of Refrigeration 2009;32:1918–28. doi:10.1016/j.ijrefrig.2009.07.006.
[51] Schiffmann J. Integrated Design and Multi-objective Optimization of a Single Stage Heat-Pump Turbocompressor. J Turbomach 2015;137:071002–071002. doi:10.1115/1.4029123.
[52] Demierre J, Favrat D, Schiffmann J, Wegele J. Experimental investigation of a Thermally Driven Heat Pump based on a double Organic Rankine Cycle and an oil-free Compressor-Turbine Unit. International Journal of Refrigeration 2014;44:91–100. doi:10.1016/j.ijrefrig.2014.04.024.
[53] Demierre J, Rubino A, Schiffmann J. Modeling and Experimental Investigation of an Oil-Free Microcompressor-Turbine Unit for an Organic Rankine Cycle Driven Heat Pump. J Eng Gas Turbines Power 2014;137:032602–032602. doi:10.1115/1.4028391.
[54] Wei D, Lu X, Lu Z, Gu J. Performance analysis and optimization of organic Rankine cycle (ORC) for waste heat recovery. Energy Conversion and Management 2007;48:1113–9. doi:10.1016/j.enconman.2006.10.020.
[55] Mago PJ, Chamra LM, Srinivasan K, Somayaji C. An examination of regenerative organic Rankine cycles using dry fluids. Applied Thermal Engineering 2008;28:998–1007. doi:10.1016/j.applthermaleng.2007.06.025.
[56] Quoilin S, Declaye S, Tchanche BF, Lemort V. Thermo-economic optimization of waste heat recovery Organic Rankine Cycles. Applied Thermal Engineering 2011;31:2885–93. doi:10.1016/j.applthermaleng.2011.05.014.
[57] Amicabile S, Lee J-I, Kum D. A comprehensive design methodology of organic Rankine cycles for the waste heat recovery of automotive heavy-duty diesel engines. Applied Thermal Engineering 2015;87:574–85. doi:10.1016/j.applthermaleng.2015.04.034.
[58] Imran M, Park BS, Kim HJ, Lee DH, Usman M, Heo M. Thermo-economic optimization of Regenerative Organic Rankine Cycle for waste heat recovery applications. Energy Conversion and Management 2014;87:107–18. doi:10.1016/j.enconman.2014.06.091.
[59] Nazari N, Heidarnejad P, Porkhial S. Multi-objective optimization of a combined steam-organic Rankine cycle based on exergy and exergo-economic analysis for waste heat recovery application. Energy Conversion and Management 2016;127:366–79. doi:10.1016/j.enconman.2016.09.022.
[60] Yang F, Zhang H, Bei C, Song S, Wang E. Parametric optimization and performance analysis of ORC (organic Rankine cycle) for diesel engine waste heat recovery with a fin-and-tube evaporator. Energy 2015;91:128–41. doi:10.1016/j.energy.2015.08.034.
[61] Galindo J, Climent H, Dolz V, Royo-Pascual L. Multi-objective optimization of a bottoming Organic Rankine Cycle (ORC) of gasoline engine using swash-plate expander. Energy Conversion and Management 2016;126:1054–65. doi:10.1016/j.enconman.2016.08.053.
[62] Bahamonde S, Pini M, De Servi C, Rubino A, Colonna P. Method for the Preliminary Fluid Dynamic Design of High-Temperature Mini-Organic Rankine Cycle Turbines. J Eng Gas Turbines Power 2017;139:082606–082606 – 14. doi:10.1115/1.4035841.
[63] Horst TA, Tegethoff W, Eilts P, Koehler J. Prediction of dynamic Rankine Cycle waste heat recovery performance and fuel saving potential in passenger car applications considering interactions with vehicles' energy management. Energy Conversion and Management 2014;78:438–51. doi:10.1016/j.enconman.2013.10.074.

[64] Battista DD, Bartolomeo MD, Villante C, Cipollone R. A Model Approach to the Sizing of an ORC Unit for WHR in Transportation Sector. SAE Int J Commer Veh 2017;10:608–17. doi:10.4271/2017-24-0159.
[65] Horst TA, Rottengruber H-S, Seifert M, Ringler J. Dynamic heat exchanger model for performance prediction and control system design of automotive waste heat recovery systems. Applied Energy 2013;105:293–303. doi:10.1016/j.apenergy.2012.12.060.
[66] Zhang HG, Wang EH, Fan BY. Heat transfer analysis of a finned-tube evaporator for engine exhaust heat recovery. Energy Conversion and Management 2013;65:438–47. doi:10.1016/j.enconman.2012.09.017.
[67] Di Battista D, Di Bartolomeo M, Villante C, Cipollone R. On the limiting factors of the waste heat recovery via ORC-based power units for on-the-road transportation sector. Energy Conversion and Management 2018;155:68–77. doi:10.1016/j.enconman.2017.10.091.
[68] Kass MD, Thomas JF, Wilson D, Lewis SA, Sarles A. Assessment of Corrosivity Associated With Exhaust Gas Recirculation in a Heavy-Duty Diesel Engine. Warrendale, PA: SAE Technical Paper; 2005.
[69] Lai NA, Wendland M, Fischer J. Working fluids for high-temperature organic Rankine cycles. Energy 2011;36:199–211. doi:10.1016/j.energy.2010.10.051.
[70] ASHRAE. ANSI/ASHRAE Standard 34-2013 Designation and Safety Classification of Refrigerants 2013.
[71] Lemmon EW, Huber ML, McLinden MO. NIST Reference Fluid Thermodynamic and Transport Properties - REFPROP Version 9.1 2013.
[72] McLinden MO, Kazakov AF, Steven Brown J, Domanski PA. A thermodynamic analysis of refrigerants: Possibilities and tradeoffs for Low-GWP refrigerants. International Journal of Refrigeration 2014;38:80–92. doi:10.1016/j.ijrefrig.2013.09.032.
[73] 3M. 3M™ Novec™ 649 Engineered Fluid. 3M n.d. https://www.3m.com/3M/en_US/company-us/all-3m-products/~/3M-Novec-649-Engineered-Fluid/?N=5002385+3290667401&rt=rud (accessed May 27, 2018).
[74] NdFeB magnets. Bomatec n.d. http://www.bomatec.com/en/products/ndfeb-magnets/ (accessed December 5, 2017).
[75] Lienhard IV JH, Lienhard V JH. A Heat Transfer Textbook. 4th Edition. Cambridge, Massachusetts, U.S.A.: Phlogiston Press; 2011.
[76] Kakaç S, Shah RK, Aung W. Handbook of single-phase convective heat transfer. Wiley; 1987.
[77] Thome JR, El Hajal J, Cavallini A. Condensation in horizontal tubes, part 2: new heat transfer model based on flow regimes. International Journal of Heat and Mass Transfer 2003;46:3365–87. doi:10.1016/S0017-9310(03)00140-6.
[78] Wojtan L, Ursenbacher T, Thome JR. Investigation of flow boiling in horizontal tubes: Part II—Development of a new heat transfer model for stratified-wavy, dryout and mist flow regimes. International Journal of Heat and Mass Transfer 2005;48:2970–85. doi:10.1016/j.ijheatmasstransfer.2004.12.013.
[79] Wojtan L, Ursenbacher T, Thome JR. Investigation of flow boiling in horizontal tubes: Part I—A new diabatic two-phase flow pattern map. International Journal of Heat and Mass Transfer 2005;48:2955–69. doi:10.1016/j.ijheatmasstransfer.2004.12.012.
[80] Balje OE. Turbomachines A Guide to Design, Selection, and Theory. New York: John Wiley & Sons, Inc.; 1981.
[81] Mounier V, Olmedo LE, Schiffmann J. Small scale radial inflow turbine performance and pre-design maps for Organic Rankine Cycles. Energy 2018;143:1072–84. doi:10.1016/j.energy.2017.11.002.

[82] Moustapha H, Zelesky MF, Baines NC, Japikse D. Axial and Radial Turbines. Concepts NREC; 2003.
[83] Fleming DPH. Optimization of self-acting herringbone journal bearings for maximum stability. 1974.
[84] Schiffmann J, Favrat D. The effect of real gas on the properties of Herringbone Grooved Journal Bearings. Tribology International 2010;43:1602–14. doi:10.1016/j.triboint.2010.03.006.
[85] Luomi J, Zwyssig C, Looser A, Kolar JW. Efficiency Optimization of a 100-W 500 #x2009;000-r/min Permanent-Magnet Machine Including Air-Friction Losses. IEEE Transactions on Industry Applications 2009;45:1368–77. doi:10.1109/TIA.2009.2023492.
[86] Hendershot Jr JR, Miller TJE. Design of Brushless Permanent-magnet Motors. Oxford, New York: Oxford University Press; 1995.
[87] Vrancik JE. Prediction of windage power loss in alternators. Cleveland, OH, USA: NASA Lewis Research Center; 1971.
[88] Hadka D, Reed P. Borg: An Auto-Adaptive Many-Objective Evolutionary Computing Framework. Evolutionary Computation 2012;21:231–59. doi:10.1162/EVCO_a_00075.
[89] Waumans T, Peirs J, Al-Bender F, Reynaerts D. Aerodynamic journal bearing with a flexible, damped support operating at 7.2 million DN. J Micromech Microeng 2011;21:104014. doi:10.1088/0960-1317/21/10/104014.
[90] Shah RK, Sekulic DP. Fundamentals of heat exchanger design. Hoboken, New Jersey: John Wiley & Sons, Inc.; 2003.